



ISSN: 0067-2904

Inelastic Form Factors for the ^{90}Zr Nucleus with Short-Range Correlations Effect

Israa Khalil. Abdalsada, Altaf A. Al-Rahmani*

Department of Physics, College of Science for Women, University of Baghdad, Baghdad, Iraq

Received: 9/6/2023

Accepted: 11/12/2023

Published: 30/12/2024

Abstract

Short-range effect on C2, C3, C4 and C5 form factors in the ^{90}Zr atomic nucleus was scrutinized. The charge density of the ^{90}Zr was as well as scrutinized via the 1- and 2-body parts of cluster expansion in collaboration with harmonic functions of single particle. To incorporate the short-range effect in the 2-body part of cluster expansion, the Jastrow formula was used. Here, the core-polarization and model space participations are what lead to the form factors in ^{90}Zr . The transition density of core polarization was calculated using the Tassie form, relying on the charge density. The elements of one body density matrix were determined by performing shell model computations using the computer code OXBASH together with the N50J interaction. The oscillator parameter b and correlation parameter β were applied to the existing calculations, where b and β are autonomously produced for each distinct nucleus by matching between the predicted and actual elastic form factors. A single value for each of b and β must be given for computing the density, elastic and inelastic form factors for diverse states in ^{90}Zr . This work provides confirmation that the short-range effect substantially dominates existing computations, where taking this effect into account appears to be crucial to creating an important modification to the predicated findings which eventually leads to a noteworthy interpretation of the data across all assumed momentum transfers.

Keywords: Electron scattering; Elastic and inelastic form factors; Nuclear density; Short-range effect; ^{90}Zr atomic nucleus; Shell model calculations

عوامل التشكل غير المرنة لنواة الزركانيوم-90 مع مراعاة تأثيرات المدى القصير

اسراء خليل عبد السادة، الطاف عبد المجيد الرحماني*

قسم الفيزياء، كلية العلوم للبنات، جامعة بغداد، بغداد، العراق

الخلاصة

تم دراسة تأثير المدى القصير على عوامل التشكل C2، C3، C4 و C5 غير مرنة في النواة الذرية ^{90}Zr . وتم أيضًا دراسة كثافة الشحنة لهذه النواة من خلال استخدام حد الجسم المنفرد وحد الجسمتين من امتداد كلاستر (Cluster expansion) وبأستخدام الدوال الموجية التوافقية للجسيم المنفرد. تم استخدام صيغة جاسترو (Jastrow formula) لأدخال تأثير المدى القصير في حد الجسمتين من امتداد كلاستر. هنا عوامل التشكل في النواة ^{90}Zr تنشأ من مساهمتين هما استقطاب القلب وأنموذج الفضاء. لقد تم حساب كثافة

*Email: altafha_phys@cs.w.uobaghdad.edu.iq

انتقال شحنة أستقطاب القلب عن طريق استخدام صيغة تاسي (Tassie form)، بالأعتماد على كثافة الشحنة. تم ايجاد عناصر مصفوفة كثافة الجسم المنفرد (OBDM) من خلال اجراء حسابات أنموذج القشرة النووي بواسطة كود الكمبيوتر OXBAH والتفاعل $N50J$. تم تطبيق معلمة المتذبذب b ومعلمة الأرتباط β ، حيث يتم توليدهما بشكل مستقل لكل نواة مميزة عن طريق المطابقة بين عوامل الشكل المرنة المتوقعة والفعلية. يجب إعطاء قيمة واحدة لكل من b و β لحساب كل من كثافة الشحنة وعوامل التشكل المرن وغير المرن لحالات متهيجة مختلفة في نواة ال ^{90}Zr . يوفر هذا العمل تأكيداً على أن التأثير قصير المدى يهيمن بشكل كبير على الحسابات الحالية، حيث يبدو أن أخذ هذا التأثير في الاعتبار أمر حاسم لإنشاء تعديل مهم للنتائج المتوقعة مما يؤدي في النهاية إلى تفسير جدير بالملاحظة للبيانات عبر جميع عمليات نقل الزخم المفترضة.

1. Introduction

In nature, the nucleus is the most intricate structure. Understanding how the short inter-particle portion of nuclear wave functions works is crucial for describing nuclei. The difficult assignment is a result of the intricate interactions between nucleons and the significant nuclear density. Additionally, understanding the work of short inter-particle portion guarantees that all crucial measurements in nuclei (for example, the mean distance, the interaction range and the nucleon size) are accurate, which makes real theoretical explanations somewhat hard [1]. The structure of the neutron [2, 3], the bound nucleon [4–8], as well as the studies of neutrino oscillations and neutrino-nucleus interactions [9–13], all depend significantly on having a complete understanding of short-range correlations (SRCs).

Present models of the average field appropriately explain a number of static characteristics [14-18] in nuclei; however, they do not succeed in explaining how the SRCs dynamic affects these characteristics. Ab-initio computations [19–22] are stagnant constrained to light nuclei with soft interactions that amend short-range parts in nuclear wave function. Accordingly, genuine models are stagnant preferred to sort the main physical technique at short distances and to interpret the mid as well as high mass nuclei [23–25].

The incorporation of SRCs into the Slater determinant was done by researches [26-28], linking universally $N = Z$ low mass nuclei from the perspective of Born approach. These researches attempted to produce a formulation for elastic form factors, $F_{el}(q)$, reduced at two particle parts using the factor cluster expansion [29-31]. This formulation was utilized to open s-, p-, and sd-nuclei as well as closed (^4He , ^{16}O and ^{40}Ca) nuclei. The influence of the SRCs on the s, p, and sd nuclei were achieved by [32] with completely differing from the strategy utilized by [26–28]. Cluster expansion and Jastrow function, which intercalates SRCs, were employed by [33] for imitating clear formulations to elastic form factors $F_{el}(q)$ and densities $\rho(r)$. In fact, these formulations hinge on the single particle motion [34-36] instead of the relative two-particle wave functions [25, 37]. It is crucial to note that the investigations stated above were exclusively concerned with the effect of SRCs on elastic $F_{el}(q)$.

Inelastic form factors $F_{inel}(q)$ with allowing for the influence of SRC's in f5p (full fp) shell nuclei, for instance $^{58-64}\text{Ni}$ ($^{46-50}\text{Ti}$, $^{50-54}\text{Cr}$, $^{54-56}\text{Fe}$ and $^{64-68}\text{Zn}$) nuclei were tested by [38] ([39]). As active protons are absent (present) in the f5p (full fp) space, the estimated $F_{inel}(q)$ in [38] ([39]) arise from the core-polarization contribution (both of the model space and core-polarization contributions).

There has been no comprehensive investigation about the effect of SRCs on $F_{inel}(q)$ outside the f5p model space. We accordingly, in this research, carry out such investigations in the N50J model space with the purpose of attain indispensable conclusions about this effect on $F_{inel}(q)$ and its connection in a dissimilar mass region, dissimilar interaction and dissimilar truncation scheme. Here, the nucleus of ^{90}Zr is chosen as a case study in the N50J model space, where the estimated results arise from the contributions of the core-polarization and model space. This research supplies confirmation that short-range effect noticeably controls existing calculations, where considering this effect is a crucial for producing a substantial amendment to the predicated findings which ultimately leads to a notable explanation of the data through all the supposed momentum transfers.

2. Theory

Inelastic form factor in electron-nucleus scattering is given by [40]:

$$|F_J^L(q)|^2 = \frac{4\pi}{Z^2(2J_i + 1)} \left| \left\langle f \parallel \hat{T}_J^L(q) \parallel i \right\rangle \right|^2 |F_{cm}(q)|^2 |F_{fs}(q)|^2, \tag{1}$$

where q is the momentum transfer, J is the angular momentum, $|i\rangle = |J_i T_i\rangle$ and $|f\rangle = |J_f T_f\rangle$ are the initial and final states labeled by $J_{i/f}$ (spin) and $T_{i/f}$ (isospin). Coulomb operator of electron-nucleus scattering is denoted by $\hat{T}_J^L(q)$, the correction of center of mass (cm) is signified by $F_{cm}(q) = e^{q^2 b^2 / 4A}$ (which is answerable for omitting untrue states made from the cm motion), the correction of finite-sized nucleon (fs) is depicted by $F_{fs}(q) = e^{-0.43q^2/4}$ (which is rumored to be equivalent for protons and neutrons), the atomic and mass numbers are represented by Z and A , correspondingly, and b is defined by $b = \sqrt{\hbar / (M_p \omega)}$ [40]. Here, $\hbar = h / 2\pi$ with h signifies the Plank's constant, M_p denotes the mass of proton and ω stands for the angular frequency. Eq. (1) may be written as [42]:

$$|F_J^L(q)|^2 = \frac{4\pi}{Z^2(2J_i + 1)} \left| \sum_{T=0,1} (-1)^{T_f - T_z} \begin{pmatrix} T_f & T & T_i \\ -T_{z_f} & 0 & T_{z_i} \end{pmatrix} \left\langle J_f T_f \parallel \hat{T}_{JT}^L(q) \parallel J_i T_i \right\rangle \right|^2 \times |F_{cm}(q)|^2 |F_{fs}(q)|^2. \tag{2}$$

In Eq. (2), the bracket stands for the 3j- symbol, T stands for the isospin and T_z stands for the isospin projection. Here T and T_z are delineated by:

$$\begin{aligned} |T_f - T_i| &\leq T \leq T_f + T_i \\ T_z &= \frac{Z - N}{2}. \end{aligned} \tag{3}$$

The reduced matrix (revealed in Eq. (2)) is specified by [41]:

$$\left\langle f \parallel \hat{T}_{JT}^L \parallel i \right\rangle = \sum_{a,b} OBDM^{JT}(i, f, J, a, b) \left\langle b \parallel \hat{T}_{JT}^L \parallel a \right\rangle, \tag{4}$$

where the symbols a and b are the single-particle states. The one-body density matrix (OBDM) is assessed using [43]:

$$\begin{aligned} OBDM(\tau_z) &= (-1)^{T_f - T_z} \begin{pmatrix} T_f & 0 & T_i \\ -T_z & 0 & T_z \end{pmatrix} \sqrt{2} \frac{OBDM(\Delta T = 0)}{2} \\ &+ \tau_z (-1)^{T_f - T_z} \begin{pmatrix} T_f & 1 & T_i \\ -T_z & 0 & T_z \end{pmatrix} \sqrt{6} \frac{OBDM(\Delta T = 1)}{2}, \end{aligned} \tag{5}$$

where τ_z symbolizes the single-particle isospin operator.

To generate the many-body reduced matrix elements of the $\hat{T}_J^L(q)$ operator, the core polarization (cp) and model space (ms) participations are added [43]:

$$\langle f \| \hat{T}_J^L(\tau_z, q) \| i \rangle = \langle f \| \hat{T}_J^L(\tau_z, q) \| i \rangle^{ms} + \langle f \| \hat{T}_J^L(\tau_z, q) \| i \rangle^{cp} \tag{6}$$

The participation of ms, in Eq. (6), is signified by:

$$\langle f \| \hat{T}_J^L(\tau_z, q) \| i \rangle^{ms} = \int_0^\infty dr r^2 j_J(qr) \rho_{J, \tau_z}^{ms}(i, f, r), \tag{7}$$

where $j_J(qr)$ stands for the spherical Bessel function whereas $\rho_{J, \tau_z}^{ms}(i, f, r)$ stands for the ms transition charge density given by [43]:

$$\rho_{J, \tau_z}^{ms}(i, f, r) = \sum_{j' \in (ms)}^{ms} OBDM(i, f, J, j, j', \tau_z) \langle j \| Y_J \| j' \rangle R_{nl}(r) R_{n'l'}(r), \tag{8}$$

where the radial and spherical components of the harmonic wave function are symbolized by $R_{nl}(r)$ and Y_J , respectively.

The participation of cp, in Eq. (6), is signified by:

$$\langle f \| \hat{T}_J^L(\tau_z, q) \| i \rangle^{cp} = \int_0^\infty dr r^2 j_J(qr) \rho_{J, \tau_z}^{cp}(i, f, r), \tag{9}$$

where the cp transition charge density $\rho_{J, \tau_z}^{cp}(i, f, r)$, which describes the nuclear collective modes, relies on the formula used for cp. Accordingly the full transition charge density owns the formulation:

$$\rho_{J, \tau_z}(i, f, r) = \rho_{J, \tau_z}^{ms}(i, f, r) + \rho_{J, \tau_z}^{cp}(i, f, r) \tag{10}$$

In this research, the $\rho_{J, \tau_z}^{cp}(i, f, r)$ is assumed to possess the formula of Tassie form [44]:

$$\rho_{J, \tau_z}^{cp}(i, f, r) = N_T \frac{1}{2} (1 + \tau_z) r^{J-1} \frac{d\rho_{ch}^{gs}(i, f, r)}{dr}, \tag{11}$$

where

$$N_T = \frac{\int_0^\infty dr r^{J+2} \rho_{\tau_z}^{ms}(i, f, r) - \sqrt{(2J_i + 1) B(CJ)}}{(2J + 1) \int_0^\infty dr r^{2J} \rho_{ch}^{gs}(i, f, r)}, \tag{12}$$

stands for the normalization constant gotten by revising of the reduced intensity $B(CJ)$ to the experimental one, and $\rho_{ch}^{gs}(i, f, r)$ stands for the ground state charge density.

For closed shell nuclei with $N = Z$, the charge density $\rho_{ch}^{gs}(r)$ can be related to the ground state density of point nucleon $\rho_p^{gs}(r)$ by:

$$\rho_{ch}^{gs}(r) = \frac{1}{2} \rho_p^{gs}(r), \quad (\text{in e.fm}^{-3}) \tag{13}$$

To accommodate the effect of SRCs into the $\rho_p^{gs}(r)$, the many-particle wave functions are expressed by:

$$\Psi = F \Phi, \tag{14}$$

where F signifies a model operator that insets SRCs and Φ signifies the Slater determinant wave function. In the existing research, F is taken as a Jastrow model [33]:

$$F = \prod_{i < j}^A f(r_{ij}), \tag{15}$$

where the two-particle SRCs, $f(r_{ij}) = f(|\vec{r}_i - \vec{r}_j|)$, are functions of state sovereign signified by: $f(r_{ij}) = 1 - \exp[-\beta(\vec{r}_i - \vec{r}_j)^2]$, (16)

and holds the features: $f(r_{ij}) \rightarrow 1$ for great amounts of $\vec{r}_{ij} = |\vec{r}_i - \vec{r}_j|$ and $f(r_{ij}) \rightarrow 0$ for $\vec{r}_{ij} \rightarrow 0$. Accordingly, the SRCs effect embedded by Eq. (16) become considerable for the low β and conversely.

A clear formula for $\rho_p^{gs}(r)$ is expressed as [32]:

$$\begin{aligned} \rho_p^{gs}(r) &= N_D \langle \Psi(\vec{r}_1, \vec{r}_2, \dots, \vec{r}_A) | \hat{O}_r | \Psi(\vec{r}_1, \vec{r}_2, \dots, \vec{r}_A) \rangle \\ &= N_D \langle \hat{O}_r \rangle. \end{aligned} \tag{17}$$

Here $\Psi(\vec{r}_1, \vec{r}_2, \dots, \vec{r}_A)$ describes the many-particle wave function shown in Eq. (14), $N_D = \langle \Psi(\vec{r}_1, \vec{r}_2, \dots, \vec{r}_A) | \Psi(\vec{r}_1, \vec{r}_2, \dots, \vec{r}_A) \rangle^{-1}$ symbolizes the normalization constant that is found by $4\pi \int_0^\infty \rho_p^{gs}(r) r^2 dr = 1$, whereas \hat{O}_r represents the density operator of one-particle that owns the formula

$$\hat{O}_r = \sum_{i=1}^A \hat{o}_r(i) = \sum_{i=1}^A \delta(\vec{r} - \vec{r}_i). \tag{18}$$

To find $\rho_p^{gs}(r)$, the generalized normalization integral was utilized [32]:

$$I(\alpha) = \langle \Psi | [\exp[\alpha I(0) \hat{O}_r] | \Psi \rangle, \tag{19}$$

similar to the operator \hat{O}_r from:

$$\langle \hat{O}_r \rangle = \left[\frac{\partial \ln I(\alpha)}{\partial \alpha} \right]_{\alpha=0}. \tag{20}$$

In cluster inquiry of Eq. (20), the integrals $I_i(\alpha), I_{ij}(\alpha) \dots$ were utilized for sectors of a system that owns A particles and a factor cluster disassembly of these integrals. The expectation value of \hat{O}_r is given by [32]:

$$\rho_p^{gs}(r) = N_D \langle \hat{O}_r \rangle = N_D \left\{ \langle \hat{O}_r \rangle_1 + \langle \hat{O}_r \rangle_2 + \dots + \langle \hat{O}_r \rangle_A \right\}, \tag{21}$$

where [32]:

$$\langle \hat{O}_r \rangle_1 = \sum_{i=1}^A \left[\frac{\partial \ln I_i(\alpha)}{\partial \alpha} \right]_{\alpha=0} = \sum_{i=1}^A \langle i | F_1^+ \hat{o}_r(1) F_1 | i \rangle, \tag{22}$$

$$\begin{aligned} \langle \hat{O}_r \rangle_2 &= \sum_{i < j}^A \frac{\partial}{\partial \alpha} [\ln I_{ij}(\alpha) - \ln I_i(\alpha) - \ln I_j(\alpha)]_{\alpha=0} \\ &= \sum_{i < j}^A \langle ij | F_{12}^+ [\hat{o}_r(1) + \hat{o}_r(2)] F_{12} | ij \rangle_a - \sum_{i < j}^A [\langle i | \hat{o}_r(1) | i \rangle + \langle j | \hat{o}_r(2) | j \rangle], \end{aligned} \tag{23}$$

and so on. Hence, the identity operator is supposed to be F_1 .

The expansion of cluster causes to fragmentation of one-particle, two- particle, . . . , A-particle correlation effects on the density. In this enquiry, more than two-particle constituents would not be utilized. Therefore, the correlated density $\rho_p^{gs}(r)$ of Eq. (21) which reflects the consequence of SRCs alters into:

$$\rho_p^{gs}(r) \approx N_D \left\{ \langle \hat{O}_r \rangle_1 + \langle \hat{O}_r \rangle_2 \right\}. \tag{24}$$

Inserting Eqs. (22) and Eq. (23) into Eq. (24), we get:

$$\rho_p^{gs}(r) \approx N_D \left\{ \sum_{i=1}^A \langle i | \hat{o}_r(1) | i \rangle + 2 \sum_{i<j}^A \langle ij | F_{12}^+ \hat{o}_r(1) F_{12} | ij \rangle_a - 2 \sum_{i<j}^A \langle ij | \hat{o}_r(1) | ij \rangle_a \right\}. \tag{25}$$

For ease, Eq. (25) is expressed in a disparate formula as:

$$\rho_p^{gs}(r) \approx N_D \left\{ \langle \hat{O}_r \rangle_1 + \langle \hat{O}_r \rangle_{22} - \langle \hat{O}_r \rangle_{21} \right\} \tag{26}$$

where

$$\langle \hat{O}_r \rangle_1 = \sum_{i=1}^A \langle i | \hat{o}_r(1) | i \rangle, \tag{27}$$

$$\langle \hat{O}_r \rangle_{22} = 2 \sum_{i<j}^A \langle ij | F_{12}^+ \hat{o}_r(1) F_{12} | ij \rangle_a, \tag{28}$$

$$\langle \hat{O}_r \rangle_{21} = 2 \sum_{i<j}^A \langle ij | \hat{o}_r(1) | ij \rangle_a, \tag{29}$$

when the two-particle SRCs of Eq. (16) are taken into account, then:

$$\begin{aligned} F_{12} F_{12} &= (1 - \exp[-\beta(\vec{r}_1 - \vec{r}_2)^2]) (1 - \exp[-\beta(\vec{r}_1 - \vec{r}_2)^2]) \\ &= 1 - 2g(r_1, r_2, \beta) + g(r_1, r_2, 2\beta) \end{aligned} \tag{30}$$

where:

$$g(r_1, r_2, z) = \exp(-z r_1^2) \exp(-z r_2^2) \exp(2z r_1 r_2 \cos w_{12}), \quad (\text{with } z = \beta \text{ or } 2\beta). \tag{31}$$

With the aid of Eqs. (30) and (31), Eq. (28) alters to:

$$\begin{aligned} \langle \hat{O}_r \rangle_{22} &= 2 \sum_{i<j}^A \langle ij | \hat{o}_r(1) [1 - 2g(r_1, r_2, \beta) + g(r_1, r_2, 2\beta)] | ij \rangle_a \\ &= 2 \left\{ \sum_{i<j}^A \langle ij | \hat{o}_r(1) | ij \rangle_a - 2 \sum_{i<j}^A \langle ij | \hat{o}_r(1) g(r_1, r_2, \beta) | ij \rangle_a + \sum_{i<j}^A \langle ij | \hat{o}_r(1) g(r_1, r_2, 2\beta) | ij \rangle_a \right\}. \end{aligned} \tag{32}$$

For ease, Eq. (32) may be expressed as:

$$\langle \hat{O}_r \rangle_{22} = \langle \hat{O}_r \rangle_{21} - 2O_{22}(r, \beta) + O_{22}(r, 2\beta), \tag{33}$$

where the two-particle fragment $O_{22}(r, z)$ is signified by:

$$O_{22}(r, z) = 2 \sum_{i<j}^A \langle ij | \hat{o}_r(1) g(r_1, r_2, z) | ij \rangle_a. \tag{34}$$

Employing Eq. (33) into Eq. (26), we obtain:

$$\rho_p^{gs}(r) \approx N_D \left\{ \langle \hat{O}_r \rangle_1 - 2O_{22}(r, \beta) + O_{22}(r, 2\beta) \right\}, \tag{35}$$

where $\rho_p^{gs}(r)$ is in need of β embedded by Eq. (16).

The one-particle fragment $\langle \hat{O}_r \rangle_1$, shown in Eq. (35), is evidently identified by:

$$\begin{aligned} \langle \hat{O}_r \rangle_1 &= \sum_{i=1}^A \langle i | \hat{\rho}_r(1) | i \rangle \\ &= 4 \sum_{nl} \eta_{nl} (2l + 1) \frac{1}{4\pi} \phi_{nl}^*(r) \phi_{nl}(r), \end{aligned} \tag{36}$$

where $\phi_{nl}(r)$ and η_{nl} designate the radial part of the single-particle wave function and the occupation probability of the state nl , in that order. By algebra of spherical harmonics, the formula of $O_{22}(r, z)$ displayed in Eq. (34) alters to [32]:

$$\begin{aligned} O_{22}(r, z) &= 4 \sum_{n_i l_i, n_j l_j} \eta_{n_i l_i} \eta_{n_j l_j} (2l_i + 1)(2l_j + 1) \\ &\times \left\{ 4 A_{n_i l_i, n_j l_j}^{n_j l_j, n_i l_i, 0}(r, z) - \sum_{k=0}^{l_i + l_j} \langle l_i 0 l_j 0 | k 0 \rangle^2 A_{n_i l_i, n_j l_j}^{n_j l_j, n_i l_i, k}(r, z) \right\}, \quad (z = \beta, 2\beta) \end{aligned} \tag{37}$$

where

$$\begin{aligned} A_{n_i l_i, n_j l_j}^{n_j l_j, n_i l_i, k}(r, z) &= \frac{1}{4\pi} \phi_{n_i l_i}^*(r) \phi_{n_j l_j}(r) \exp(-zr^2) \\ &\times \int_0^\infty \phi_{n_2 l_2}^*(r_2) \phi_{n_4 l_4}(r_2) \exp(-zr_2^2) i_k(2zrr_2) r_2^2 dr_2, \end{aligned} \tag{38}$$

with $\langle l_i 0 l_j 0 | k 0 \rangle$ and $i_k(x)$ symbolize the Clebsch Gordan coefficient and the modified spherical Bessel function, respectively.

In reality, Eqs. (13) to (38) are suggested for $Z = N$ closed-shell nuclei with $\eta_{nl} = 0$ or 1. For $Z \neq N$ open-shell nuclei, an identical formulas can as well be utilized but using $0 \leq \eta_{nl} \leq 1$.

The mean square radii is demarcated by:

$$\langle r^2 \rangle = \frac{4\pi}{Z} \int_0^\infty \rho_{ch}^{gs}(r) r^4 dr, \tag{39}$$

where

$$Z = 4\pi \int_0^\infty \rho_{ch}^{gs}(r) r^2 dr, \tag{40}$$

is the normalization constant of $\rho_{ch}^{gs}(r)$.

Note that $F_{el}(q)$ is accompanying with $\rho_{ch}^{gs}(r)$, where $F_{el}(q)$ is fundamentally the Fourier transform of $\rho_{ch}^{gs}(r)$. i.e.:

$$F_{el}(q) = \frac{4\pi}{Z} \int_0^\infty \rho_{ch}^{gs}(r) j_0(qr) r^2 dr \tag{41}$$

Taking into account the corrections $F_{cm}(q)$ as well as $F_{fs}(q)$ in Eq. (41), we obtain:

$$F_{el}(q) = \frac{4\pi}{Z} \int_0^\infty \rho_{ch}^{gs}(r) j_0(qr) r^2 dr F_{cm}(q) F_{fs}(q) \tag{42}$$

3. Results and discussion

The calculations of charge density $\rho_{ch}^{gs}(r)$, elastic $F_{el}(q)$ and inelastic $F_{inel}(q)$ form factors in ^{90}Zr nucleus were performed. Two classes of calculations were achieved using single-particle wave functions of harmonic potential without (class-1) and with (class-2) the

effect of SRCs. The calculations of class-1 are reliant only on b but those in class-2 are reliant on b and β . The magnitudes of b and β in class-1 (class-2), displayed in Table 1, were created by amending b in an effort to match the calculated rms radius β and $(b < r_{ch}^2 >_{cal.}^{1/2}$ (the $< r_{ch}^2 >_{cal.}^{1/2}$ and the calculated $F_{el}(q)$)) with those of experimental data. The quantities of $< r_{ch}^2 >_{exp}^{1/2}$ [45], $< r_{ch}^2 >_{cal.}^{1/2}$ and the partaking of SRCs, $< r^2 >_{2-body}^{1/2} = \sqrt{< r_{ch}^2 >_{cal.} - < r_{ch}^2 >_{1-body}}$, to the $< r_{ch}^2 >_{cal.}^{1/2}$ of ^{90}Zr nucleus are also displayed in Table 1. In reality, Table 1 illustrates that b has an inequity relation: $b(\text{class-1}) > b(\text{class-2})$, where the addition of SRCs increases the relative distance amid nucleons which successively makes an upsurge in the size of the nucleus. As a result, it is necessary to shorten the value of b that goes along with the nuclear size (which was experimentally steady).

Table 1: The yielded magnitudes of b , β and the partaking of one- particle and two-particle charge densities to the total rms charge radius $< r_{ch}^2 >_{cal.}^{1/2}$ of ^{90}Zr nucleus. Class-1 specifies the calculations of one-particle fragment (without the effect of SRCs) whereas class-2 specifies the calculations of one-particle in addition to the two-particle fragments (with the effect of SRCs).

Class	b (fm)	β (fm ²)	Calculated rms charge radius $< r_{ch}^2 >_{cal.}^{1/2}$ (fm)			Experimental rms radius $< r_{ch}^2 >_{exp.}^{1/2}$ (fm)
			No SRCs effect (one-body part) $< r_{ch}^2 >_{1-body}^{1/2}$	With SRCs effect (two-body part) $< r_{ch}^2 >_{2-body}^{1/2}$	Total rms radius $< r_{ch}^2 >_{cal.}^{1/2}$	
1	2.25	0	4.2918	0	4.2918	4.28±0.002 [45]
2	2.02	1.75	3.8981	1.7805	4.2855	

In Figure 1, the $F_{el}(q)$ [Fig. 1(a)] and $\rho_{ch}^{gs}(r)$ [Fig. 1(b)] in the ^{90}Zr nucleus calculated without SRCs (the dashed curve) and with SRCs (the solid curve) are revealed as well as compared with the measured results (open circle symbols).

In Fig. 1(a), the calculated outcomes of $F_{el}(q)$ are plotted against the momentum transfer q (fm⁻¹). At $q < 0.8$ fm⁻¹, both outcomes of class-1 (the dashed curve) and class-2 (the solid curve) are in well accord with the measured results. Moreover, the data is manifestly under predicted (over predicted) by the dashed curve at momentum transfer $0.8 \leq q \leq 2.5$ ($q > 2.5$) fm⁻¹. Comprising the effect of SRCs (the solid curve) upsurges the magnitudes of $F_{el}(q)$ at all considered momentum transfer which sequential causes to put them into the place of consistency with the measured results.

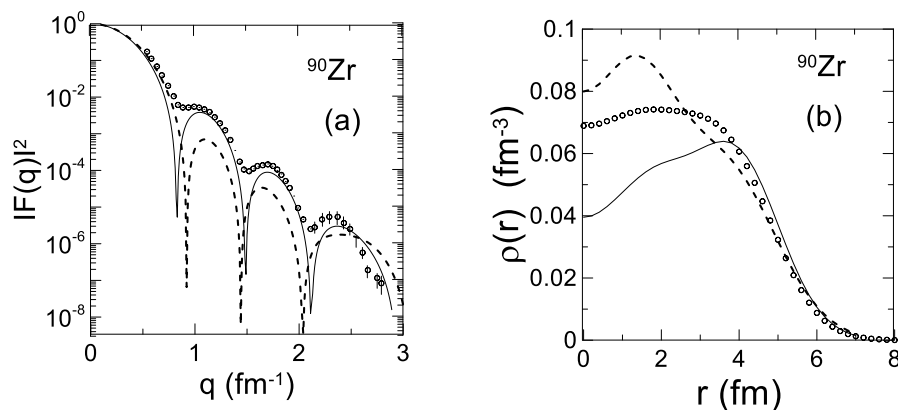


Figure 1: Square of elastic form factors $F_{el}(q)$ [Fig. 1(a)] and the charge density distribution $\rho_{ch}^{gs}(r)$ [Fig. 1(b)] in the ^{90}Zr nucleus. The dashed and solid curves are the calculated outcomes of class-1 (without SRCs) and class-2 (with SRCs), correspondingly. The experimental data (open circle symbols) is taken in (a) and (b) from [46] and [45], respectively.

In Fig. 1(b), the charge density distribution $\rho_{ch}^{gs}(r)$ is plotted versus r . It is apparent from this figure that there is a higher chance of finding a proton nearby the central segment of $\rho_{ch}^{gs}(r)$ than that of the tail segment. In addition, the implanting of SRCs into the calculations of class-2 (the solid curve) leads to diminish substantially the central segment of $\rho_{ch}^{gs}(r)$ and at the same time leads to upsurge slightly the tail segment of $\rho_{ch}^{gs}(r)$. This provides the explication that the addition of SRCs leads to increase the likelihood of shifting the protons from central segment of the nucleus towards its surface which in turn causes to rise the rms radius of the studied nucleus and makes it less rigid than it would be in the absence of the SRC's effect. To retain the size of studied nucleus within the steady observed magnitude, the parameter b has to be abridged when permitting for the influence of SRC's.

Next, the influence of SRCs on inelastic form factors $F_{inel}(q)$ for dissimilar states in the ^{90}Zr is argued. It is believed that this nucleus made up of an inert core having a neutron magic number (50 neutrons) at the orbital $1g_{9/2}$ and a proton magic number (28 protons) at the orbital $1f_{7/2}$ as well as 12 active protons spread in the N50J-model space, defined by the orbitals $2p_{3/2}$, $1f_{5/2}$, $2p_{1/2}$ and $1g_{9/2}$. The inelastic form factors in the ^{90}Zr nucleus come up from $\rho_{J\tau_z}^{ms}(i, f, r)$ and $\rho_{J\tau_z}^{cp}(i, f, r)$ transition charge densities. The quantity $\rho_{J\tau_z}^{ms}(i, f, r)$ is found by Eq. (8) while the quantity $\rho_{J\tau_z}^{cp}(i, f, r)$ is found by Tassie model of Eq. (11) in collaboration with the $\rho_{ch}^{gs}(r)$, where $\rho_{ch}^{gs}(r)$ is calculated by Eq. (13) in common with Eqs. (35) - (38). The OBDM elements of N50J-space, where mixing of configurations is considered, are found through carrying out shell calculations utilizing the OXBASH-program together with the N50J interaction [47]. The form factors $F_{inel}(q)$ of dissimilar states in ^{90}Zr are estimated employing a single magnitude for each of b and β , where these magnitudes (exposed in Table 1) are yielded by matching the calculated elastic form factors $F_{el}(q)$ and rms charge radius $\langle r_{ch}^2 \rangle_{Cal}^{1/2}$ with those of experimental data.

The comparison between the predicted and experimental $F_{inel}(q)$ in ^{90}Zr nucleus is displayed in Figs. 2-5, where all considered transitions are of an isovector in nature (i.e., $T \neq 0$). Note that the nucleus of ^{90}Zr has $T=6$. In these figures, the open circle symbols

denote the experimental results [48] while the dashed and solid curves denote class-1 and class-2 predictions gotten without and with the enhancement of SRCs effect, congruently.

The C2 form factors $F_{inel.}(q)$ in ^{90}Zr nucleus for electric quadrupole transitions from an initial state $J_i = 0^+$ to final states $J_f = 2^+$ are presented in Fig. 2, where the parity of these transitions remains the same amid the initial and final states.

In Fig. 2(a), the C2 outcomes for $0^+ \rightarrow 2^+$ transition (with excitation energy $E_x = 2.186$ MeV and reduced transition probability $B(C2) = 673 \pm 59 e^2 \cdot \text{fm}^4$ [48]) are displayed. Actually, the state 2.186 MeV is the strongest one among those of observed 2^+ states and was observed in the region of momentum transfer $0.64\text{-}1.72 \text{ fm}^{-1}$ [48]. It is noticeable that the C2 results estimated without the effect of SRCs under predict slightly (noticeably) the data at momentum transfer region $q \leq 0.9$ ($q > 0.9$) fm^{-1} . Inserting of the effect of SRCs into class-2 computations causes to enhance the C2 outcome which in turn takes the solid curve into location of agreement with the data over the regions of $q \leq 0.9$ and $q \geq 1.1 \text{ fm}^{-1}$. It is so clear that the influence of SRCs is not operative at the range $0.9 < q < 1.1 \text{ fm}^{-1}$, where both the dashed and solid curves are coincide with each other and thus the data is not reproduced well by these curves at this region of q . Additionally, the solid curve accurately reproduces the performance of the experimental C2 results along the first and second diffraction minima and maxima. Fig 2(a) shows that the effect of SRCs becomes larger at the second loop than that at the first loop.

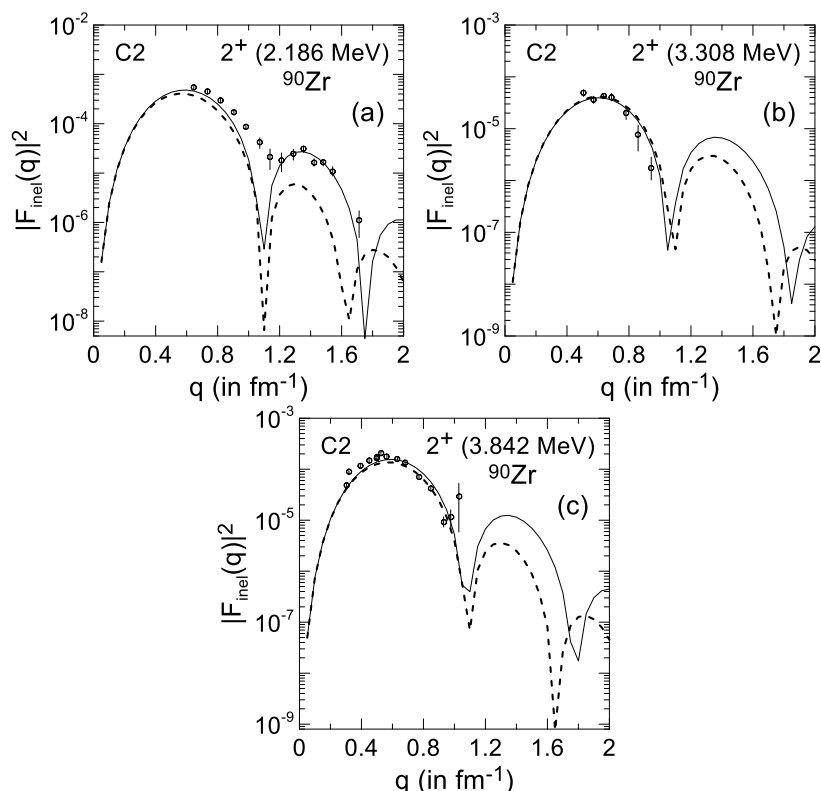


Figure 2: Square of inelastic C2 form factors for 2^+ (2.186 MeV) (Fig. 2(a)), 2^+ (3.308 MeV) (Fig. 2(b)) and 2^+ (3.842 MeV) (Fig. 2(c)) states in the ^{90}Zr nucleus. The dashed and solid curves are the calculated outcomes of class-1 (without SRCs effect) and class-2 (with SRCs effect), respectively. The experimental data of open circle symbols in (a), (b) and (c) is taken from [48].

In Fig. 2(b) (Fig. 2(c)), the C2 results for $0^+ \rightarrow 2^+$ transition ($E_x = 3.308$ MeV, $B(C2) = 69 \pm 18 e^2 \cdot \text{fm}^4$) ($E_x = 3.842$ MeV, $B(C2) = 206 \pm 36 e^2 \cdot \text{fm}^4$) [48] are displayed. In fact, the state 3.308 (3.842) MeV was measured in the momentum transfer range from 0.53 to 0.95 (0.3 to 1.06) fm^{-1} [48]. It is manifest that the open circle symbols (the measured data) are very well predicted by those of the dashed (class-1) and solid curves (class-2). The manners of the dashed and solid curves are in very good accord with those of open circle symbols. The C2 results in Fig. 2(b) (Fig. 2(c)) demonstrate that the effect of SRCs, which represents the strength of the contrast between the dashed and solid curves, is the larger at the second loop than that of the first loop. Moreover, Fig. 2(a, b and c) reveals that the considering of SRCs effect in class-2 calculations (the solid curve) leads to shift the second minimum towards the higher momentum transfer q .

The C3 form factors in ^{90}Zr nucleus for electric octupole transitions from an initial state $J_i = 0^+$ to final states $J_f = 3^-$ are exposed in figure (3), where the parity of these transitions does not remain the same amidst the initial and final states.

In Fig. 3(a), the C3 form factors for $0^+ \rightarrow 3^-$ transition ($E_x = 2.748$ MeV, $B(C3) = (8.74 \pm 1.0) \times 10^4 e^2 \cdot \text{fm}^6$) [48] are exposed. In reality, the state 2.748 MeV is the sturdiest one amongst those of observed 3^- states and was detected in momentum transfer regions 0.326-1.06 fm^{-1} [46] and 0.648-1.73 fm^{-1} [48]. It is perceptible that the C3 outcomes computed without the influence of SRCs (the dashed curve) agrees well the data at $q < 0.6 \text{ fm}^{-1}$ and undervalues clearly the data at $q \geq 0.6 \text{ fm}^{-1}$. Embedding of the influence of SRCs into class-2 calculations causes to augment the C3 outcomes, which consecutive leads to fetch the results of the solid curve into the location of consistency with the observed data considered in the studies [48, 49]. This figure also demonstrates that the presentation of the observed data (open circle symbols) alongside the first and second diffraction maxima, and alongside the first diffraction minimum are very well reestablished by the class-2 computations (the solid curve). Again, this figure demonstrates that the influence of SRCs is the bigger at the second loop than that of the first loop.

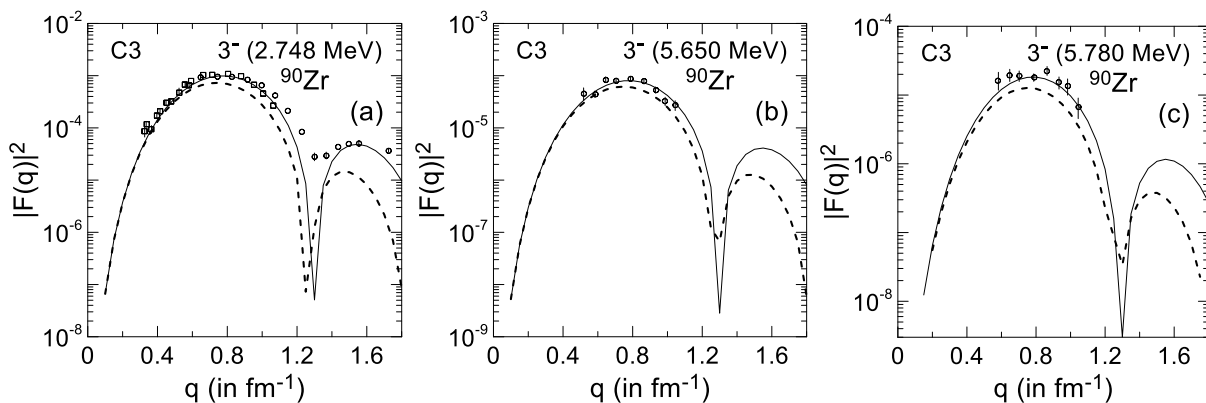


Figure 3: Same as in Fig. 2 but for C3 inelastic form factors. In (a) the data of open circle and open square symbols are taken from [48] and [49], respectively whereas in (b) and (c) the data of open circle symbols are taken from [48].

In Fig. 3(b) (Fig. 3(c)), the C3 outcomes for $0^+ \rightarrow 3^-$ transition ($E_x = 5.65$ MeV, $B(C3) = 6760 \pm 950 e^2 \cdot \text{fm}^6$) ($E_x = 5.78$ MeV, $B(C3) = 1450 \pm 220 e^2 \cdot \text{fm}^6$) [48] are exposed. Indeed, the state 5.65 (5.78) MeV was measured in the momentum transfer range from 0.51 to 1.05

(0.58 to 1.05) fm^{-1} [48]. It is patent from this figure that the dashed curve, which defines the computations of class-1 (without SRCs effect), underestimates somewhat the measured data of open circle symbols. Taking into consideration of SRCs effect by the computations of class-2 leads to reinforce the C3 outcomes (the solid curve) which sequential causes to transport the solid curve into the locus of agreement with the measured data through all considered region of q values. Furthermore, the behavior of measured C3 form factors is very well regenerated by the solid curve. Once more, this figure proves that the influence of SRCs becomes more strength at the second loop than that of the first loop.

The C4 form factors in ^{90}Zr nucleus for transitions from the state $J_i = 0^+$ to final states $J_f = 4^+$ are revealed in figure (4). It is obvious that the parity in these transitions does not change between the initial and final states.

In Fig. 4(a), the C4 form factors for $0^+ \rightarrow 4^+$ transition ($E_x = 3.077$ MeV, $B(\text{C4}) = (2.95 \pm 0.80) \times 10^5 \text{ e}^2 \cdot \text{fm}^8$) [48] are revealed. The excitation of the 3.077 MeV level was observed in q - ranges 0.66-1.06 fm^{-1} [48] and 0.81-1.73 [50]. It is visible that the C4 outcomes evaluated without imbedding of SRCs underestimates clearly the data across the entire q values considered in this study. Imbedding of the SRCs into class-2 computations leads to enlarge the C4 outcomes, which consecutively makes the solid curve in good (reasonable) contract with the data at $q \leq 1.06$ ($q > 1.06$) fm^{-1} . Fig. 4(a) also proves that the performance of the experimental results (open circle symbols) alongside the first and second diffraction maxima as well as along with the first diffraction minimum are very well reconstructed by the class-2 calculations (the solid curve).

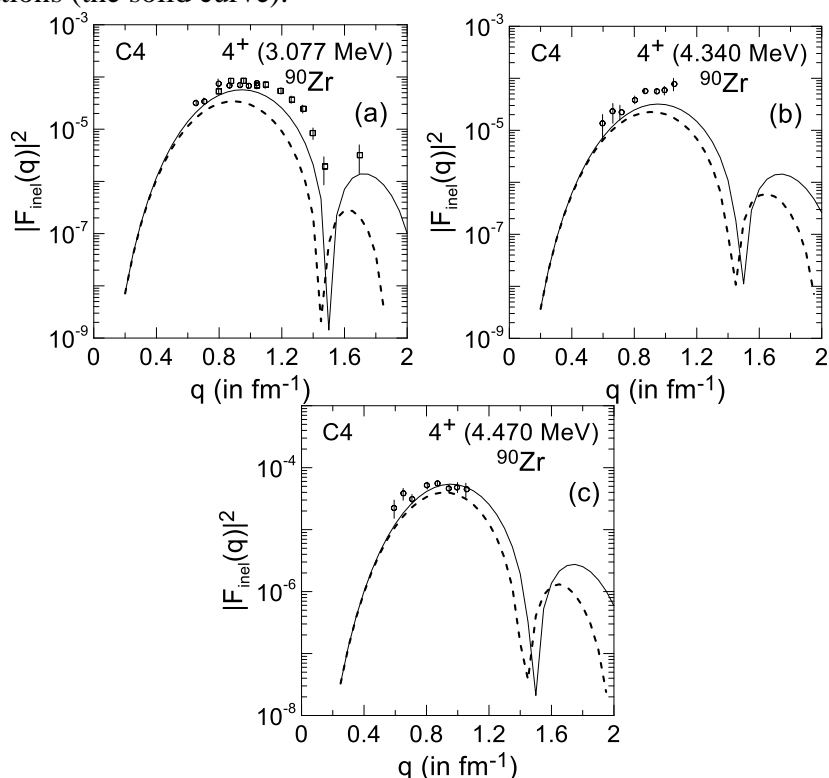


Figure 4: Same as in Fig. 2 but for C4 inelastic form factors. In (a) the data of open circle and open square symbols are taken from [48] and [50], respectively while in (b) and (c) the data of open circle symbols are taken from [48].

In Fig. 4(b) (Fig. 4(c)), the C4 form factors for $0^+ \rightarrow 4^+$ transition ($E_x = 4.34$ MeV, $B(C4) = (1.5 \pm 0.40) \times 10^5$ e².fm⁸) ($E_x = 4.47$ MeV, $B(C4) = (3.45 \pm 0.65) \times 10^5$ e².fm⁸) [48] are revealed. Undeniably, the level 4.34 (4.47) MeV was identified in the momentum transfer region from 0.59 to 1.06 fm⁻¹ [48]. It is clear from Fig. 4(b) (Fig. 4(c)) that the dashed curve, which signifies the class-1 computations (without SRCs), underrates visibly (slightly) the data at the entire considered q values. Inclusion of the SRCs effect by class-2 computations leads to strengthen the C4 results (the solid curve) throughout all considered q values which consecutively takes the solid curve into the site of closer (concurrence) with the data (open circle symbols). Additionally, the manner of experimental C4 form factors is superbly re-created by the solid curve of class-2 computations. Again, this figure demonstrates that the SRCs come to be more operative over the second loop than that of the first loop.

The C5 form factors in ⁹⁰Zr nucleus for transitions from an initial state $J_i = 0^+$ to final states $J_f = 5^-$ are seen in figure (5), where the parity of these transitions alters amongst the initial and final states.

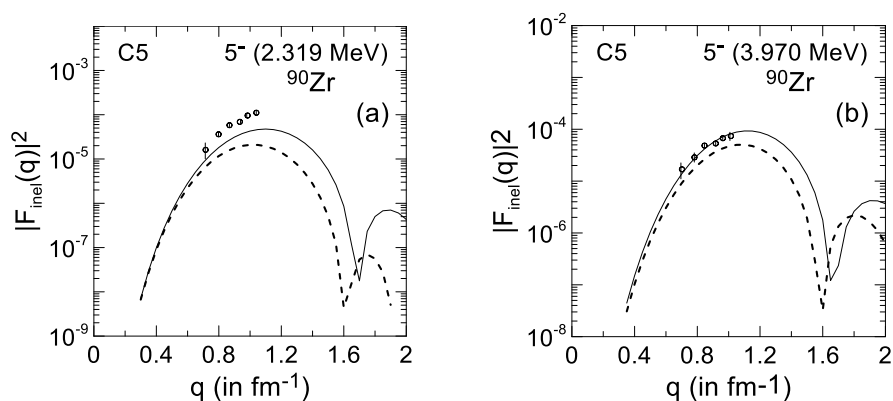


Figure 5: Same as in Fig. 2 but for C5 inelastic form factors. The experimental data in (a) and (b) is taken from [48].

In Figure 5(a) (Fig. 5(b)), the C5 form factors for $0^+ \rightarrow 5^-$ transition ($E_x = 2.319$ MeV, $B(C5) = (2.12 \pm 0.12) \times 10^7$ e².fm¹⁰) ($E_x = 3.97$ MeV, $B(C5) = (2.62 \pm 1.00) \times 10^7$ e².fm¹⁰) [48] are shown. Definitely, both states 2.319 and 3.97 MeV were observed in the q - range from 0.71 to 1.06 fm⁻¹ [48]. It is evident from Fig. 5(a) (Fig. 5(b)) that the dashed curve, which indicates the calculations when there is no the influence of SRCs, underrates perceptibly (somewhat) the data across all considered q -values. Inserting of SRCs effect by the calculation of solid curves leads to support the outcomes of C5 across the whole considered q - values which consecutively brings the solid curve into the location of nearer (agreement) with the experimental data (open circle symbols). Moreover, the behaviors of experimental C5 form factors are wonderfully re-formed by the solid curve of class-2 calculations. For a second time, this figure exhibits that the SRCs become more effective throughout the second loop than that of the first loop.

4. Conclusions

This work presents the conclusion that the short-range correlations effect noticeably controls the existing calculations, as taking this effect into consideration seems to be crucial in establishing a significant alteration in the predicated findings which ultimately leads to a noteworthy explanation of the data throughout the studied region of momentum transfer. In

addition, this effect becomes more operative across the higher momentum transfer of the second loop than that of the first loop.

Acknowledgment

The authors would like to give their gratitude to Professor B.A. Brown of the National Super-conducting Cyclotron Laboratory, Michigan State University, for providing the OXBASH-code.

References

- [1] R.Weiss, R.Cruz-Torres, N.Barnea, E.Piasetzky, O.Hen, "The nuclear contacts and short range correlations in nuclei," *Physics Letters B*, vol. 780, pp. 211–215, 2018.
- [2] O. Hen, B. A. Li, W.-J. Guo, L.B. Weinstein, E. Piasetzky, "Symmetry energy of nucleonic matter with tensor correlations," *Physical review C*, vol. 91, no. 2, pp. 25803-25815, 2015.
- [3] B.-J. Cai, B. A. Li, "Symmetry energy of cold nucleonic matter within a relativistic mean field model encapsulating effects of high-momentum nucleons induced by short-range correlations," *Physical Review C*, vol. 93, no. 1, pp. 14619-14633, 2016.
- [4] L.B. Weinstein, E. Piasetzky, D.W. Higinbotham, J. Gomez, O. Hen, R. Shneor, "Short range correlations and the EMC effect," *Physical Review Letters*, vol. 106, no. 5, pp. 52301-52306, 2011.
- [5] O. Hen, A. Accardi, W. Melnitchouk, E. Piasetzky, "Constraints on the large-x d/u ratio from electron-nucleus scattering at $x > 1$," *Physical Review D*, vol. 84, no. 11, pp. 117501-117517, 2011.
- [6] O. Hen, D.W. Higinbotham, G.A. Miller, E. Piasetzky, L.B. Weinstein, "The EMC effect and high momentum nucleons in nuclei," *Int. J. Mod. Phys. E*, vol. 22, no. 7, pp. 1330017-1330029, 2013.
- [7] O. Hen, G.A. Miller, E. Piasetzky, L.B. Weinstein, "Nucleon-nucleon correlations, short-lived excitations, and the quarks within," *Rev. Mod. Phys.*, vol. 89, no. 4, pp. 45002-45015, 2017.
- [8] O. Hen, E. Piasetzky, L.B. Weinstein, "New data strengthen the connection between short range correlations and the EMC effect," *Phys. Rev. C*, vol. 85, no. 4, pp. 47301-47319, 2012.
- [9] H. Gallagher, G. Garvey, G.P. Zeller, "Neutrino-nucleus interactions," *Ann. Rev. Nucl. Part. Sci.*, vol. 61, pp. 355-378, 2011.
- [10] L. Fields, J. Chvojka, L. Aliaga, O. Altinok, B. Baldin, A. Baumbaugh, A. Bodek, et al., "Measurement of muon antineutrino quasielastic scattering on a hydrocarbon target at $E_{\nu} \sim 3.5$ GeV," *Phys.Rev. Lett.*, vol. 111, no. 2, pp. 22501-22506, 2013.
- [11] G.A. Fiorentini, D.W. Schmitz, P.A. Rodrigues, L. Aliaga, O. Altinok, B. Baldin, A. Baumbaugh, et al., "Measurement of muon neutrino quasielastic scattering on a hydrocarbon target at $E_{\nu} \sim 3.5$ GeV," *Phys.Rev. Lett.*, vol. 111, no. 2, pp. 22502-22511, 2013.
- [12] R. Acciarri, C. Adams, J. Asaadi, B. Baller, T. Bolton, C. Bromberg, F. Cavanna, et al., "The detection of back-to-back proton pairs in charged-current neutrino interactions with the ArgoNeUT detector in the NuMI low energy beam line," *Phys. Rev. D*, vol. 90, pp. 12008-12021, 2014.
- [13] L.B. Weinstein, O. Hen, E. Piasetzky, "Hammer events, neutrino energies and nucleon-nucleon correlations," *Phy. Rev. C*, vol. 94, no. 4, pp. 45501-45517, 2016.
- [14] Altaf A Al-Rahmani and S F Kazem, "Elastic electron-nucleus scattering form factors of selected medium mass nuclei," *NeuroQuantology*, vol. 18, no. 8, pp.: 49-58, 2020.
- [15] Altaf Abdul Majeed Al-Rahmani and Huda Abd Aljabbar Hussein, "Elastic Electron Scattering form Factors for odd-A 2s-1d Shell Nuclei," *Iraqi Journal of Science*, vol. 55, no. 4B, pp. 1868-1875, 2014.
- [16] F. I. Sharrad, A K Hamoudi, R A Radhi, H Y Abdullah, "Inelastic electron scattering from light nuclei," *J.Natn. Sci. Foundation Sri Lanka*, vol. 41 pp. 209-217, 2013.
- [17] A. A. M. Al-Rahmani, "Charge density distributions for odd-A of 2s-1d shell nuclei," *Baghdad Science Journal*, vol 7, no. 2, pp 1028-1033, 2010.
- [18] Altaf Abdul Majeed Al-Rahmani, "Elastic Form Factors and Proton Momentum Distributions From Some fp shell Nuclei Using the Coherent Density Fluctuation Model," *Iraqi Journal of Science*, vol. 57, no. 3A, PP. 1688-1698, 2016.

- [19] R.B. Wiringa, R. Schiavilla, S.C. Pieper, J. Carlson, "Nucleon and nucleon-pair momentum distributions in $A \leq 12$ nuclei," *Phys. Rev. C*, vol. 89, no. 2, pp. 24305-24321, 2014.
- [20] J. Carlson, S. Gandolfi, F. Pederiva, S.C. Pieper, R. Schiavilla, K.E. Schmidt, R.B. Wiringa, "Quantum Monte Carlo methods for nuclear physics" *Reviews of Modern Physics*, vol. 87, no. 3, pp. 1067-1079, 2015.
- [21] G. Hagen, A. Ekström, C. Forssén, G. R. Jansen, W. Nazarewicz, et al., "Neutron and weak-charge distributions of the ^{48}Ca nucleus," *Nat. Phys.*, vol. 12, no. 2, pp. 186–190, 2016.
- [22] D. Lonardoni, A. Lovato, S.C. Pieper, R.B. Wiringa, "Variational calculation of the ground state of closed-shell nuclei up to $A = 40$," *Phys. Rev. C*, vol. 96, no.2, pp. 24326-24338, 2017.
- [23] J. Ryckebusch, M. Vanhalst, W. Cosyn, "Stylized features of single-nucleon momentum distributions," *Journal of Physics G, Nucl. Part. Phys.*, vol. 42, no. 5, pp. 55104-55123, 2015.
- [24] M. Vanhalst, J. Ryckebusch, W. Cosyn, "Quantifying short-range correlations in nuclei," *Phys. Rev. C*, vol. 86, no. 4, pp. 44619-44635, 2012.
- [25] C. Colle, O. Hen, W. Cosyn, I. Korover, E. Piasezky, J. Ryckebusch, L.B. Weinstein, "Extracting the mass dependence and quantum numbers of short-range correlated pairs from $A(e, e' p)$ and $A(e, e' p p)$ scattering," *Phys. Rev. C*, vol. 92, no. 2, pp. 24604-24618, 2015.
- [26] S.E. Massen, H.P. Nassen and C.P. Panos, "A formula for the charge form factor of closed-shell nuclei and its application to ^{16}O ," *J. Phys. G*, vol. 14, pp. 753-764, 1988.
- [27] S.E. Massen and C.P. Panos, "An approximate treatment of the correlated charge form factor of light nuclei," *J. Phys. G: Nucl. Phys*, vol. 15, pp. 311-319, 1989.
- [28] S.E. Massen, "Correlated charge form factor and densities of the s-d shell nuclei," *J. Phys. G: Nucl. Phys*, vol. 16, pp. 1713-1725, 1990.
- [29] J.W. Clark and M.L. Ristig, "Cluster-Expansion Procedures for the Correlated Charge Form Factor," *Nuovo Cimento A*, vol. 70, pp. 313-322, 1970.
- [30] M.L. Ristig, W.J. Ter Low, J.W. Clark, "Tensor Correlations in Nuclear Matter," *Phys. Rev. C*, vol. 3, pp. 1504-1513, 1971.
- [31] W. Clark, "Variational theory of nuclear matter," *Prog. Part. Nucl. Phys.*, vol. 2, pp. 89-99, 1979.
- [32] S.E. Massen and Ch. C. Moustakidis, "Systematic study of the effect of short range correlations on the form factors and densities of s-p and s-d shell nuclei," *Phys. Rev. C*, vol. 60, pp. 24005-24017, 1999.
- [33] R. Jastrow, "Many-Body Problem with Strong Forces," *Phys. Rev.*, vol. 98, pp. 1479-1484, 1955.
- [34] Adel K Hamoudi and Mahmoud A. Abbas, "Electron scattering from some even fp-and N50-shell nuclei with implanting the influence of short-range correlation functions," *Chinese Journal of Physics*, vol. 60, pp. 623-631, 2019.
- [35] Adel K Hamoudi and Mahmoud A. Abbas, "Electron scattering from some fp-shell nuclei with inclusion the effect of short-range correlation," *Iraqi Journal of Science*, vol. 61, no. 10, pp. 2540-2550, 2020.
- [36] Adel K Hamoudi and Abdullah S. Mdekil, "The effect of short range correlation on the nuclear charge density distribution, elastic and inelastic electron scattering coulomb form factors of ^{18}O nucleus," *Iraqi Journal of Science*, vol. 56, no. 4A, pp. 2867-2879, 2015.
- [37] F.I. Sharrad, A.K. Hamoudi, R.A. Radhi, Hewa Y. Abdullah, A.A. Okhunov and H. Abu Kassim, "Elastic Electron Scattering from Some Light Nuclei," *Chinese Journal of Physics*, vol. 51, pp. 452-465, 2013.
- [38] Mahmoud A Abbas and Adel K Hamoudi, "Elastic and inelastic C2 form factors of nickel isotopes and two-body correlations," *International Journal of Modern Physics E*, vol. 30, no. 10, pp. 2150080- 2150094, 2021.
- [39] Sanna N. Fadhil, Sarrah I. Abdalsattar and Altaf A. Al-Rahmani, "Proof for strong ascendancy of short range effects on inelastic form factors in some open fp-shell nuclei," *International Journal of Modern Physics E*, vol. 31, no. 9, pp. 2250087-1 (16 pages), 2022.
- [40] B.A. Brown, B.H. Wildenthal, C.F. Williamson, F.N. Rad, S. Kowalski, Hall Crannell, J.T. Brien, "Shell-model analysis of high-resolution data for elastic and inelastic electron scattering on ^{19}F ," *Physical Reviews C*, vol. 32, pp. 1127–1156, 1985.
- [41] P.J. Brussard and P.W.M. Glaudemans, *Shell-Model Applications in Nuclear Spectroscopy*, North Holland, Amsterdam, 1977, p. 14.

- [42] T.W. Donnelly and I. Sick Rev., "Elastic magnetic electron scattering from nuclei," *Rev. Mod. Phys.*, vol. 56, pp. 461–566, 1984.
- [43] B. A. Brown, R. Radhi and B.H. Wildenthal, "Electric quadrupole and hexadecupole nuclear excitations from the perspectives of electron scattering and modern shell-model theory," *Phys. Rep.*, vol. 101, pp. 313–358, 1983.
- [44] L. J. Tassie, "A Model of Nuclear Shape Oscillations for E2 Transitions and Electron Excitation," *Austr. J. Phys.*, vol. 9, pp. 407-413, 1956.
- [45] H. De Vries, C.W. De Jager, and C. De Vries, "Nuclear charge density distribution parameters from elastic electron scattering," *Atomic Data and Nuclear Data Tables*, vol. 36, pp. 495-536, 1987.
- [46] L. A. Fajardo, J. R. Ficenec, W. P. Trower, and I. Sick. "Elastic electron – Zirconium scattering," *Phys. Lett.*, vol. 37 B, no. 4, pp. 363-365, 1971.
- [47] B. A. Brown, A. Etchegoyen, N. S. Godwin, W.D.M. Rae, W. A. Richter, W. E. Ormand, E. K. Warburton, J. S. Winfield, L. Zhao, C. H. Zimmerman, "Oxbash Code for Windows PC, MSU-NSCL report number 1289, 2005. For information on obtaining a copy contact the author at: brown@nscl.msu.edu.
- [48] R. P. Singhal, S. W. Brain, C. S. Carrant, W. A. Gillespie, A. Johnston, E. W. Lees and A. G. Slight, "Inelastic scattering of electrons from ^{90}Zr ," *J. Phys. G: Nucl. Phys.*, vol. 1, no. 5, pp. 558-578, 1975.
- [49] J. Bellicard, P. Leconte, T. H. Curtis, R. A. Eisenstein, and D. Madsen, "The scattering of 60 MeV electrons from ^{90}Zr ," *Nucl. Phys. A*, vol. 143, Issue 1, pp. 213-224, 1970.
- [50] Phan-Xuan-Ho, J. Bellicard, P. Leconte, and I. Sick, "Inelastic electron scattering from even single-closed-shell nuclei," *Nucl. Phys. A*, vol. 210, Issue 1, pp. 189-210, 1973.